CAUCHY – Jurnal Matematika Murni dan Aplikasi
Volume 10 (2) (2025), Pages 957-969
p-ISSN: 2086-0382; e-ISSN: 2477-3344

# A Hybrid ARIMA-Intervention Modelling for Forest Fire Risk in The Dry Season

Nurfitri Imro'ah[1*], Nur'ainul Miftahul Huda[2], Hesty Pratiwi[1], and Muhammad Yahya Ayyash[1]

[1] *Department of Statistics, Universitas Tanjungpura, Indonesia*
[2] *Department of Mathematics, Universitas Tanjungpura, Indonesia*

**Abstract**

This study explores the time-related patterns of forest fires and assesses the impact of measures implemented during the dry season. The novelty of this study lies in integrating intervention factors into the ARIMA model and combining temporal analysis with spatial data to evaluate how mitigation efforts influence both the frequency and intensity of fires. Special focus is directed towards the effects of these interventions on the frequency and intensity of fires. This study highlights the importance of combining temporal analysis with spatial data to identify high-risk locations and optimize resource allocation for fire prevention. This study develops an ARIMA model to forecast fire risk before intervention. The findings indicate that integrating intervention factors into the ARIMA model will enhance the model's accuracy. The satisfactory MAPE values and the value data plots effectively demonstrate the data patterns. This method establishes a solid basis for predicting and reducing the risk of forest fires in the dry season, thereby enhancing the fire resilience of ecosystems considered at risk. The findings indicate that the onset of the dry season significantly elevates the risk of forest fires, especially in areas near bodies of water.

**Keywords:** Accuracy; ARIMA Model; Grid; Step Function



## 1 Introduction

Forest fires have been a persistent and widespread environmental problem for a long time in Indonesia, an archipelago that is well-known for the lush tropical forests that it contains [1]. Both human health and the environment are faced with significant dangers due to these fires, which affect nearly 70 million hectares of forest yearly. It is important to note that the impact of these fires is diverse and far-reaching. They have caused enormous harm to ecosystems, released massive amounts of carbon dioxide into the atmosphere, and affected millions of people through respiratory ailments. Land conversion for agricultural use and plantations, particularly the expansion of palm oil plantations, is the principal factor that contributes to forest fires in Indonesia. Peatlands rich in carbon material become highly combustible due to draining them, making the problem much worse [2]. The frequency and severity of these fires have also been linked to climate change, which has been identified as a significant factor in both areas. Forest fires are a persistent environmental issue that occurs annually in Indonesia, with most of these

[*]**Corresponding author**. E-mail: nurfitriimroah@math.untan.ac.id

Submitted: September 01, 2025 Reviewed: September 17, 2025 Accepted: October 13, 2025
DOI: https://doi.org/10.18860/cauchy.v10i2.36741

occurring on the island of Kalimantan. One of them is a forest fire in the province of West Kalimantan.

The province of West Kalimantan is situated on the westernmost portion of the island of Kalimantan [3]. Based on the map, it is between 2°08′ north latitude and 302‘ south latitude and between 108°30 to 114°10 east longitude. West Kalimantan is an area traversed by the equator or the line located at a latitude of 0°. Because of this, the temperature and humidity levels in the region are among the highest in the world. Additionally, the region is home to vast tropical forests and an abundance of unique and numerous species. However, the facts about the natural condition of West Kalimantan are concerning because forest fires frequently occur and recur from year to year [4]. According to information provided by the Regional Disaster Management Agency of West Kalimantan Province, 322 villages and sub-districts are at risk of losing their forests and land to fire. Ketapang Regency is home to 45 villages and subdistricts that are particularly vulnerable to forest and land fires at any given time. According to the information provided by Manggala Agni, the total area of land and forest that was destroyed by fire in Ketapang for the past six years reached 91,388.00 hectares in 2019. By the year 2020, this number has significantly fallen to 1,843.00 hectares. Because of the increase in the number of cases of COVID-19, there was a decrease in the amount of land that humans burned. However, this number will go up again between 2021 and 2023, reaching a total of 43,561.91 hectares.

The Ketapang Regency is in around 14 Peat Hydrological Areas, which collectively cover an area of approximately 151,590 hectares of peat domes. Peat is a type of soil generated from the accumulation of plant remains that have been partially decomposed; hence, the amount of organic matter present in peat is exceptionally high. This material is buried deep within the earth and can be found at a depth of up to four meters. If the conditions of the fire triangle are met, fire may be produced. Three components comprise the fire triangle: oxygen (O2), fuel, and a heat source. There is a significant amount of organic material in peatlands, typically places where plants can flourish. The abundance of organic matter and a plentiful supply of oxygen both contribute to the susceptibility of peatlands to experience fire [5]. When it comes to agricultural land, most of the peat land in Ketapang is utilized. Considering this, the likelihood of forest and land fires increasing due to land clearing through burning increases. When the dry season begins, the region of peatlands spread out across Ketapang Regency is one of the major weaknesses that could be exposed to forest and land fires. If a fire breaks out on peatland, putting it out will be highly challenging [6]. When a fire breaks out on the peatland's surface, it can spread to the deeper layers of the bog, making it more difficult to detect. Additionally, the fire has the potential to travel to other places through the interior of the peatland. Even though the fire has been doused on the surface, the interior of the peatland still contains hotspots. This is because the wetland contains a large quantity of organic material. There is a greater likelihood of these hotspots forming during the dry season [7].

The relatively dry weather and air conditions are the root reason for the rise in the number of hot spots. These conditions cause plants to become combustible, which drives the increase. During the prolonged dry season, hot spots become more prevalent [8]. There is a rise in the influence of this dry season, which extends to several different locations. There are hot spots, which are indicators of forest or land fires that are discovered from a location that has a temperature that is relatively high in comparison to the temperature of the surrounding area as well as regions that, according to temperature thresholds, are monitored by satellites, have a surface temperature that is higher than the temperature of the surrounding area. To identify hot areas, the Meteorology, Climatology, and Geophysics Agency frequently makes use of satellite data [9]. This is because satellite data serves as an early predictor of forest and land fires in an area. Within a region that is one-kilometer square, the satellite will identify temperature anomalies that are abnormally high. It will be witnessed anywhere from two to four times every day at a particular spot on the surface of the planet. The detection of hotspots is impossible in regions that are shrouded by clouds. There are additional secondary causes that contribute

to the dispersion of hot spots, such as drought and severe wind gusts. Reflexivity and ambient temperature anomalies are the only things that are evaluated by satellite imaging, and these differences are interpreted as hot areas [10].

Low (indicator code 0-29%), medium (indicator code 30-79%), and high (indicator code 80-100%) are the tiers of confidence that are assigned to hot spots. These tiers are based on the indicator codes. The systematic level of certainty regarding fire is that which is referred to as the hot spot confidence level. A hotspot, for instance, has a confidence level of 80%, which indicates that it is possible to conclude that the certainty that the hotspot is genuine is 80% [11]. The confidence is directly proportional to the degree of certainty that the hot spot is as it should be. The ability to accurately predict the level of confidence associated with hotspots is essential for developing successful fire management and prevention methods. Understanding these levels can reduce the danger of catastrophic wildfires by minimizing the risk of focused interventions and resource allocation. If stakeholders use modern forecasting tools, they can better plan for wildfires and limit their effects.

From the point of view of temporal analysis, this research aims to investigate forest fire cases, with a particular emphasis on the degree of confidence in fire hotspots, by incorporating intervention elements. During this investigation, the dry season in West Kalimantan served as the intervention. Therefore, this research can give significant insights regarding the temporal dynamics of forest fires and the effectiveness of interventions during the dry season, which will ultimately lead to the development of forest management techniques that are more robust in the face of climate change. The data utilized in this investigation was gathered from NASA satellites as confidence-level data for hotspots centered in Ketapang Regency between January 2019 and December 2023. During this investigation, the dry season was selected as an intervention, and it was subsequently incorporated into the modeling process utilizing temporal analysis. In this model, the target variable represents the number of detected hotspots over time, while the intervention variable reflects the implementation of mitigation measures during the dry season. These specifications are essential for accurately evaluating the temporal impact of interventions on fire occurrence.

## 2 Methods

One of the most significant concepts for prediction is time series analysis. This theory is beneficial in fields where data is gathered over time, and it is necessary to identify patterns or trends. The analysis in question is a valuable instrument in geography, as it enables researchers to discover patterns, trends, and cyclical behavior in spatial data over time. Applications of this technology can be found in various sectors, including climate studies, environmental studies, and disaster studies. Several studies that use temporal analysis in the context of forest fires include predicting the incidence of flames ([12], [13], [14]), tracking the spread of fires ([15], [16], [17]), and forecasting risks ([18], [19]).

In the case of forest fires, several occurrences occur, each leading to a dramatic increase or drop in the average. One would refer to this as an intervention. The advent of the dry season is one intervention that can be considered in this situation. Suppose this intervention is not taken into consideration throughout the analysis. In that case, the model created will result in relatively significant errors, indicating that the prediction's accuracy level is deficient. It is, therefore, impossible to consider the findings of the analysis while deciding. Because of this, adding intervention elements to the investigation is of the utmost importance.

### 2.1 ARIMA Time Series Model

One type of non-stationary time series model is known as the ARIMA model. Its general form can be either the Autoregressive (AR) or Moving Average (MA) model or a combination of the

two, which is referred to as the ARMA model. The applied ARIMA model is defined by three orders: $p$, $d$, and $q$ [20]. The order of the AR model is $p$, the order of the MA model is $q$, and the order of the differentiation process is $d$. Consequently, the ARIMA model can be expressed as ARIMA $(p, d, q)$ in its general form [21].

$$\phi_p(B)(1-B)^d Y_t = \theta_q(B)e_t \tag{1}$$

where

$$\phi_p(B) = (1 - \phi_1 B - \cdots - \phi_p B^p), \quad \theta_q(B) = (1 - \theta_1 B - \cdots - \theta_q B^q),$$

$B$ is the Backshift Operator, and $e_t$ is the error at time $t$.

Three basic procedures include time series modeling. A study of the patterns that are seen in the Autocorrelation Function (ACF) and the Partial Autocorrelation Function (PACF) is used to pick the orders of $(p, d, q)$ in the ARIMA model. It represents the process's first stage, known as model identification. Methods commonly used, such as the Maximum Likelihood Estimation (MLE) and the Ordinary Least Squares (OLS), are utilized in the second stage, which is the estimation of parameters. Tests for residual white noise and residual normality are included in the diagnostic testing of the model's residual, which is the final stage of the process. Three major stages are followed by selecting the optimal model, which is then utilized as a point of reference to forecast the future [22].

## 2.2 Intervention Factor-Based ARIMA Model

Two types of time series models include intervening factors: pulse function $P_t^{(T)}$ and step function $S_t^{(T)}$. An intervention with a step function takes place at time $T$ and has a lasting effect. A pulse function is an intervention that has no effect outside of the time it has an effect, either before or after $t = T$. The two intervention types are [23]:

$$S_t^{(T)} = \begin{cases} 0, & \text{for } t < T \\ 1, & \text{for } t \geq T \end{cases} \qquad P_t^{(T)} = \begin{cases} 0, & \text{for } t \neq T \\ 1, & \text{for } t = T \end{cases}$$

Interventions involving step and pulse can elicit a wide variety of responses. The responses to interventions that frequently occur are [24]:

1. During the $b$ period following the intervention, its ongoing impact manifests itself: $\omega B^b S_t^{(T)}$ or $\omega B^b P_t^{(T)}$. For those who are utilizing the step function, the intervention will have a constant influence on $\omega$; however, for those who are utilizing the pulse function, the intervention will only impact $\omega$ during the moment when the event occurs, which is $T$.
2. The step function is written as the perceived influence of the intervention in the period after the intervention; however, the response or effect that results from the intervention is gradual [25]:

   $$\frac{\omega B^b}{1 - \delta B} S_t^{(T)},$$

   and for the pulse function:

   $$\frac{\omega B^b}{1 - \delta B} P_t^{(T)},$$

   where $0 \leq \delta \leq 1$. An intervention based on the step function will have an impact that continues to gradually increase or decrease until its effect reaches constancy. An intervention based on the pulse function will have an impact that is gradual, but the impact produced will converge to zero, which means that it will come to an end at a specific time [26].

When modeling time series with intervening factors, it is essential to consider the mechanisms that can induce changes or the implied effects of the anticipated changes to determine the design of the intervention model. To evaluate the form of intervention effects that are attributable to

known events, direct inspection of the data can facilitate identification. In the case of intervening factors, the general ARIMA$(p, d, q)$ model $\{Y_t\}$ is [27]:

$$Y_t = f_t + N_t$$

where $f_t = \frac{\omega_c(B)}{\delta_r(B)} B^b I_t^{(T)}$ and $N_t$ is the time series model before adding intervention factors; $B$ is the Backshift Operator; $I_t^{(T)}$ is the intervention variable (step function or pulse function); and $\omega_c(B) = 1 - \omega_1 B - \cdots - \omega_c B^c, \quad \delta_r(B) = 1 - \delta_1 B - \cdots - \delta_r B^r$.

## 3 Results and Discussion

As confidence level data for hotspots located on Ketapang Regency (see Fig. 1a), the data used in this inquiry was obtained from NASA satellites between January 2019 and December 2023, when it was collected. The method of processing the data started with the creation of six grids that were centered in the Ketapang Regency (see Fig. 1b). After that, data processing continued to determine intervention points for each grid. Before the intervention, the initial modeling takes place with the data. The data were then subjected to stationarity testing, which was performed on the collected data's mean and variance. The data is treated to a differencing or transformation procedure until it is stationary in terms of mean and variance. It occurs if the data is not fulfilled stationary prior to the process. After that, the procedure continues with identifying the order based on the ACF and PACF plots derived from the stationary data. The procedure proceeds with parameter estimates and residual diagnostic tests, which must satisfy the assumptions of residual independence and residual normality (white noise). It occurs after the probability of the model being built has been considered. The next stage, which is to select the best model based on the smallest AIC value, is to determine whether these two assumptions are correct. The back-to-order identification process goes if the residual does not satisfy these presumptions.


**(a)** **(b)**

**Figure 1:** Research location

After the intervention factors were added to the ARIMA model, the process of estimating the parameters of the ARIMA model with intervention factors and evaluating the intervention effect was carried out. To ensure that the assumptions of residual independence and normalcy are fulfilled, the intervention ARIMA model that was obtained will then be subjected to a residual diagnostic testing procedure. The ARIMA model, with the addition of intervention factors, is the best model to use if it can satisfy these two assumptions. Fig. 2 presents a concise explanation of the flowchart that represents the research.

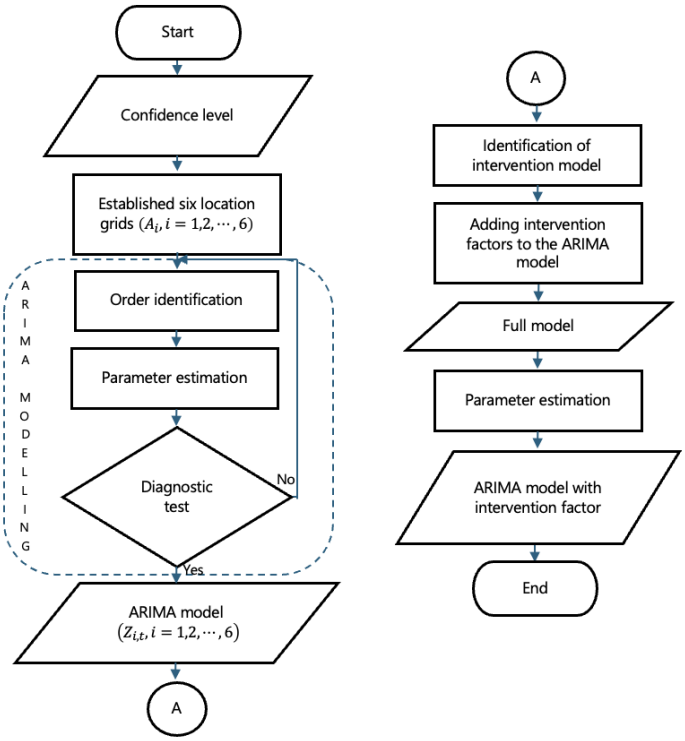


**Figure 2:** Flowchart of the research

The data that was utilized in this study was hotspot confidence level data that was concentrated in Ketapang Regency from January 2019 to December 2023. A total of sixty observations were made during the months that were used. The initial step was to establish six grids using the Ketapang Regency as their center (referred to as grids A1, A2, A3, A4, A5, and A6). Each grid calculates the maximum confidence level value for each month. As a result, the data that is acquired and examined corresponds to the confidence level data for hotspots monthly. In this study, only one intervention is utilized, and that is when the dry season occurs (July 2023) or when the temperature is 55 degrees. When modeling time series with intervention factors, the first thing that must be done is to classify the data from before and after the intervention; in this study, the pre-intervention data began in January 2019 and continued until June 2023. The data are presented in the form of descriptive statistics in Table 1 and time series charts in Figure 3, respectively. In the pre-intervention data, it is clear from Table 1 that the average confidence level of hotspots is higher than the median. It indicates that there is a positive skewness, which indicates that the confidence level of hotspots has been growing monthly since the intervention. The post-intervention data exhibits negative skewness, which indicates that the average is lower than the median. It indicates that the confidence level of hotspots is dropping, which is inversely proportional to the relationship between the two. On the other hand, the level of confidence did not immediately diminish following the intervention; rather, the value increased for several months before beginning to decline (see Fig. 3). In addition, Fig. 4 clearly shows that the average level of confidence for hotspots is consistently high throughout September, with a range between 90 and 100.

**Table 1:** Numerical Summary

| | **Minimum** | **Median** | **Mean** | **Range** | **Maximum** |
|---|---|---|---|---|---|
| Pre-intervention | 12 | 50.75 | 52.95 | 87.67 | 100 |
| Post-intervention | 14 | 91.00 | 75.08 | 85.17 | 99 |

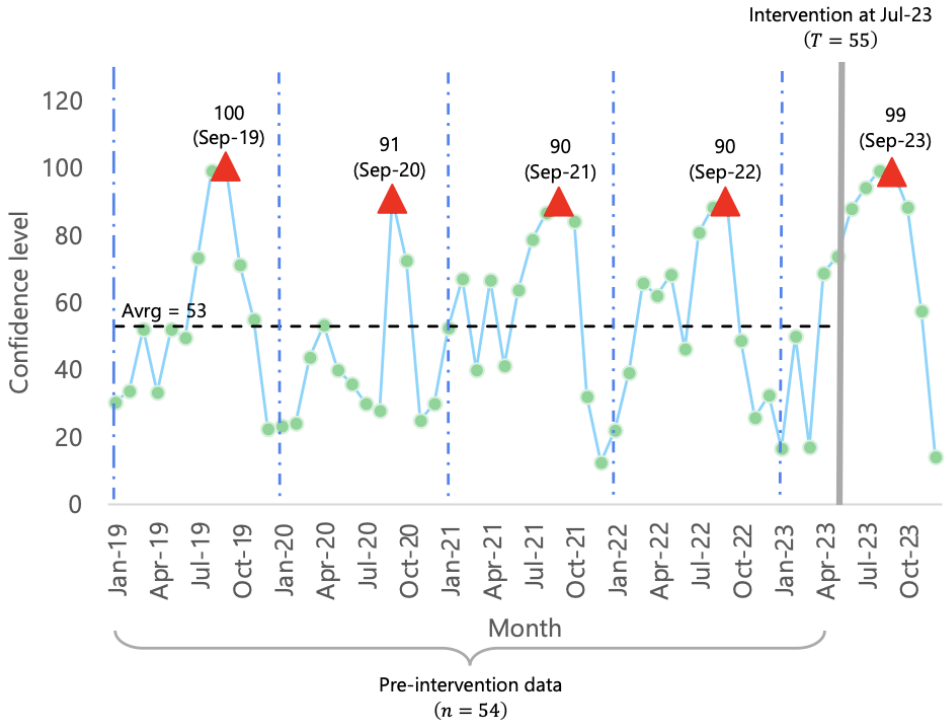


**Figure 3:** Time series plot

The advent of the dry season (the intervention in this research) generates changes in the form of an average increase in the confidence level of hotspots, based on Table 1. It suggests that the intervention itself has an impact or effect, so it is interesting to note that intervention factors should not be ignored in time series modeling, particularly the ARIMA model. Fig. 4 depicts the geographic division of the six location grids used in this investigation. Then, the ARIMA model was utilized to analyze the maximum confidence level value for each grid. Before the intervention, 54 observations were used to construct the ARIMA model. Table 2 displays the results of the ARIMA modeling performed on each grid. According to Table 2, the ARIMA models that are the most suitable $\forall A_i;\ i = 1, 2, \ldots, 6$ are sequentially: ARIMA (0,0,1), ARIMA (2,0,1), ARIMA (1,1,0), ARIMA (0,0,1), ARIMA (1,1,0), and ARIMA (0,1,1).

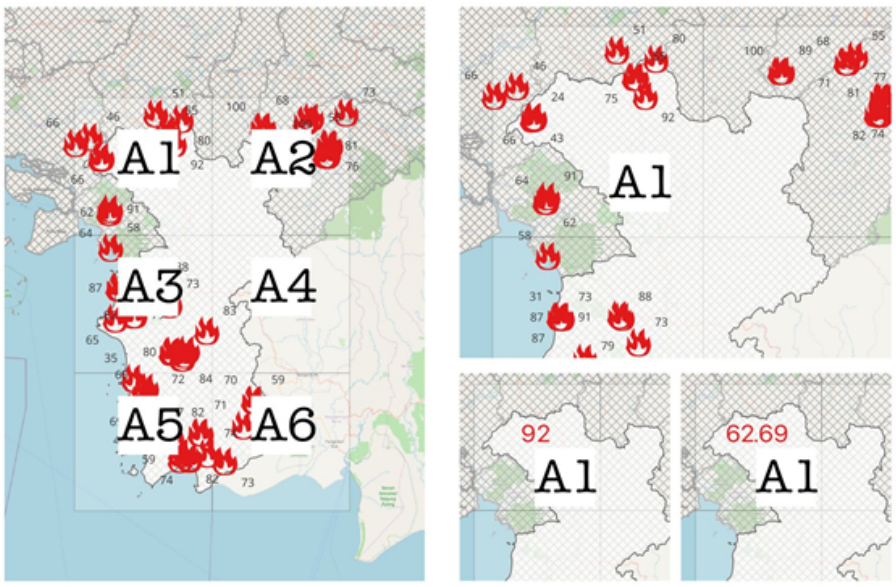


**Figure 4:** The illustration of the confidence levels of hotspots over six grids

**Table 2:** Parameter Estimation for pre-intervention data

| Grid | Order $(p,d,q)$ | Parameter estimation | | Residuals plot | AIC | MSE | MAE |
|---|---|---|---|---|---|---|---|
| A1 | $(0,0,1)$ | $\theta_1$ | 0.4371 | 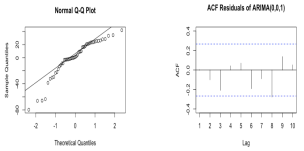 | 512.34 | 377.45 | 14.98 |
| A2 | $(2,0,1)$ | $\phi_1$<br>$\phi_2$<br>$\theta_1$ | 1.2336<br>-0.5346<br>-0.8373 | 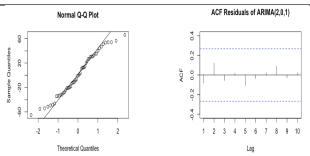 | 544.43 | 790.99 | 23.28 |
| A3 | $(1,1,0)$ | $\phi_1$ | -0.4677 | 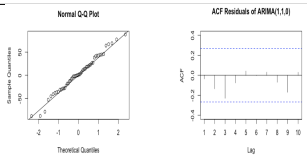 | 544.00 | 886 | 23.39 |
| A4 | $(0,0,1)$ | $\theta_1$ | 0.4021 | 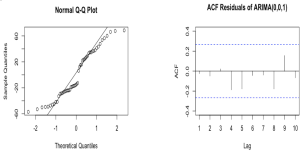 | 547.95 | 710 | 24.44 |
| A5 | $(1,1,0)$ | $\phi_1$ | -0.3879 | 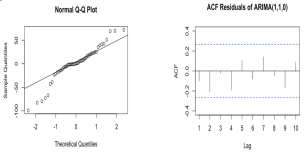 | 532.82 | 572 | 19.29 |
| A6 | $(0,1,1)$ | $\theta_1$ | -0.4274 | 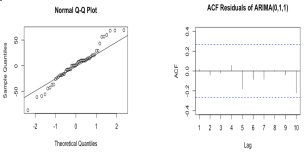 | 526.18 | 309 | 14.96 |

In the process of modeling time series with intervention variables in hotspot level confidence modeling, the intervention model that was selected based on the study of data behavior and the type of intervention that was carried out is

$$f_{55}(\omega,\delta) = \frac{\omega B}{1-\delta B} S_t^{(55)} \tag{2}$$

The intervention that takes place in July 2023 is modeled after Eq. 2. This model has a delay effect equal to a one-time lag. A step function is utilized in this model to reflect the fact that the advent of a dry season will have a permanent impact. As a result, the complete model of time series modeling consisting of intervention factors in this research is

$$Y_t = \frac{\omega B}{1-\delta B} S_t^{(55)} + N_t$$

where $N_t$ is the best ARIMA model for each grid. As an illustration, for grid $A_1$:

$$Y_t = \frac{\omega B}{1-\delta B} S_t^{(55)} + e_t - \theta_1 e_{t-1},$$
$$Y_t(1-\delta B) = \omega B S_{t-1}^{(55)} + e_t - \delta B e_t - \theta_1 e_{t-1} + \delta\theta_1 B e_{t-1}.$$

**Table 3:** Parameter estimation for full model

| Grid | Parameter estimation | | MAPE (%) | Plot of actual vs fitted values |
|---|---|---|---|---|
| A1: | $Y_t = \delta_1 Y_{t-1} + \omega S_{t-1}^{(55)} + (-\delta_2 - \theta_1)e_{t-1} + \delta_3\theta_1 e_{t-2} + e_t$ | | | |
| | $\omega$ | **2.1619** | 14 |  |
| | $\delta_1$ | 1.1738 | | |
| | $(-\delta_2 - \theta_1)$ | -0.6884 | | |
| | $(\delta_3\theta_1)$ | 0.6054 | | |
| A2: | $Y_t = \omega S_{t-1}^{(55)} + (\delta + \phi_1)Y_{t-1} + (\phi_2 - \delta\phi_1)Y_{t-2} + (-\delta\phi_2)Y_{t-3} + e_t$ $+ (-\theta_1 + \delta)e_{t-1} + (\delta\theta_1)e_{t-2}$ | | | |
| | $\omega$ | **13.7916** | 16 | 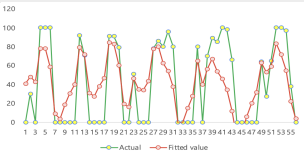 |
| | $(\delta + \phi_1)$ | 0.6816 | | |
| | $(\phi_2 - \delta\phi_1)$ | 0.4584 | | |
| | $(-\delta\phi_2)$ | -0.5001 | | |
| | $(\theta_1 + \delta)$ | -0.3422 | | |
| | $(\theta_1\delta)$ | -0.6931 | | |
| A3: | $Y_t = \omega S_{t-1}^{(55)} + (1 + \delta + \phi_1)Y_{t-1} + (-\phi_1 - \delta - \phi_1\delta)Y_{t-2} + (\phi_1\delta)Y_{t-3}$ $+ e_t + (-\theta_1 - \delta)e_{t-1} + (\theta_1\delta)e_{t-2}$ | | | |
| | $\omega$ | **31.5495** | 21 |  |
| | $(1 + \delta + \phi_1)$ | -4,264,727.5 | | |
| | $(-\phi_1 - \delta - \phi_1\delta)$ | 2,301,621.31 | | |
| | $(\phi_1\delta)$ | 1,963,106.27 | | |
| | $(-\theta_1 - \delta)$ | 4,264,727.74 | | |
| | $(\theta_1\delta)$ | 0.1208 | | |
| A4: | $Y_t = \delta_1 Y_{t-1} + \omega S_{t-1}^{(55)} + (-\delta_2 - \theta_1)e_{t-1} + \delta_3\theta_1 e_{t-2} + e_t$ | | | |
| | $\omega$ | **19.4579** | 15 | 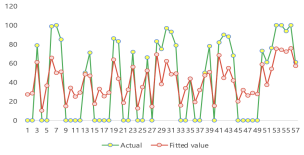 |
| | $\delta_1$ | 0.8271 | | |
| | $(-\delta_2 - \theta_1)$ | -0.4045 | | |
| | $(\delta_3\theta_1)$ | -0.4172 | | |
| A5: | $Y_t = \omega S_{t-1}^{(55)} + (1 + \delta + \phi_1)Y_{t-1} + (-\phi_1 - \delta - \phi_1\delta)Y_{t-2} + (\phi_1\delta)Y_{t-3}$ $+ e_t + (-\theta_1 - \delta)e_{t-1} + (\theta_1\delta)e_{t-2}$ | | | |
| | $\omega$ | **-0.36805** | 15 | 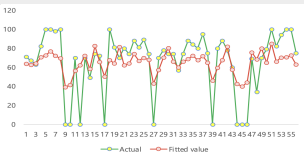 |
| | $(1 + \delta + \phi_1)$ | -893,935.4 | | |
| | $(-\phi_1 - \delta - \phi_1\delta)$ | 568,604.591 | | |
| | $(\phi_1\delta)$ | 325,330.942 | | |
| | $(-\theta_1 - \delta)$ | 893,935.686 | | |
| | $(\theta_1\delta)$ | 0.1208 | | |
| A6: | $Y_t = \omega S_{t-1}^{(55)} + (1 + \delta)Y_{t-1} + (-\delta)Y_{t-2} + e_t + (-\theta_1 - \delta)e_{t-1} + (\theta_1\delta)e_{t-2}$ | | | |
| | $\omega$ | **-1.9339** | 11 | 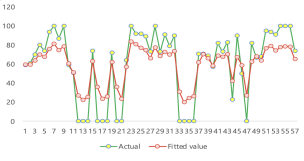 |
| | $(1 + \delta)$ | -0.2669 | | |
| | $(-\delta)$ | 0.7905 | | |
| | $(-\theta_1 - \delta)$ | 0.7564 | | |
| | $(\theta_1\delta)$ | -0.2097 | | |

therefore, the full model for grid $A_1$ is

$$Y_t = \delta_1 Y_{t-1} + \omega S_{t-1}^{(55)} + (-\delta_2 - \theta_1)e_{t-1} + \delta_3\theta_1 e_{t-2} + e_t.$$

Table 3 presents a tabular representation of the complete model for the entire grid. The parameters estimated using the Least Square approach are represented by the blue text in Table 3. The outcomes of these parameter estimations are in the second column of Table 3, which is in the document. Meanwhile, the third and fourth columns present the MAPE values and plot actual data vs. fitted values.

Table 3 also reveals that the mean absolute percentage error (MAPE) value for all grids is 15.33%. It indicates that the model's accuracy, which considers intervening circumstances, is considered "good" for predicting the confidence level that hotspots would have throughout the subsequent few periods. Aside from that, the degree of the effect resulting from adding the intervention element can be observed in the bold language presented in Table 3. Take, for instance, the value of omega on grid A3: 31.5495. It demonstrates that by the end of the dry season, there was a change of 31.5495 in the confidence level of hotspots in grid A3, and this impact will continue to be noticed ever since the dry season. Grid A3 is the grid affected the most by the intervention compared to the other grids. Based on Fig. 4, the placement of grid A3 is situated in a region close to a river (water). The peat surface in places close to rivers dries off rapidly during the dry season. When dry, peat is highly flammable, making it an ideal option for starting fires in forests. Because peat is combustible, the rapid drying of the peat surface increases the likelihood of hotspots. It is because peat causes fire to spread rapidly. Furthermore, regions near rivers frequently feature a combination of land uses, such as agricultural land and peatlands. The high frequency of dry events that occur more frequently during the dry season is partially responsible for the frequent occurrence of hotspots in certain regions during the dry season. Additionally, the same argument applies to various grids.

## 4 Conclusion

The beginning of the dry season in Indonesia, which is in July 2023, will affect the confidence level of hotspots in several different regions, including Ketapang Regency. According to the results of six grids that were constructed at places that were centered in Ketapang Regency, the grids that are placed near water are the ones that experience the greatest impacts because of the dry season. The rapid drying of the peat surface is the cause of this phenomenon, which raises the risk of forest fires occurring during the dry season. The dry season is crucial for monitoring and avoiding forest fires because of the existing conditions. This study uses temporal analysis, particularly the ARIMA model, to construct the ARIMA model before the intervention, which will take place during the dry season in July of 2023. Based on the MAPE values obtained, incorporating intervention factors into the ARIMA model results in a satisfactory level of accuracy. It is also possible to observe this from the fitted value data plot, which accurately depicts the pattern of the real data.

## CRediT Authorship Contribution Statement

**Nurfitri Imro'ah:** Conceptualization, Methodology, Writing-Original Draft. **Nur'ainul Miftahul Huda:** Data Curation, Formal Analysis, Writing–Review & Editing. **Hesty Pratiwi:** Software, Visualization. **Muhammad Yahya Ayyash:** Software, Project Administration.

## Declaration of Generative AI and AI-assisted technologies

No generative AI or AI-assisted technologies were used during the preparation of this manuscript.

## Declaration of Competing Interest

The authors declare no competing interests.

## Funding and Acknowledgments

This research received no external funding.

## Data and Code Availability

The data and code supporting the findings of this study are available from the corresponding author upon reasonable request and subject to confidentiality agreements.

## References

[1] S. Sloan, L. Tacconi, and M. E. Cattau, "Fire prevention in managed landscapes: Recent success and challenges in indonesia," *Mitigation and Adaptation Strategies for Global Change*, vol. 26, no. 7, pp. 32–32, 2021. DOI: 10.1007/s11027-021-09965-2.

[2] I. D. Rotherham, *Peatlands*. Routledge, 2020. DOI: 10.4324/9780429439285.

[3] J. Supriatna et al., "Deforestation on the indonesian island of sulawesi and the loss of primate habitat," *Global Ecology and Conservation*, vol. 24, e01205, 2020. DOI: 10.1016/j.gecco.2020.e01205.

[4] D. Arisanty, M. Muhaimin, D. Rosadi, A. N. Saputra, K. P. Hastuti, and I. Rajiani, "Spatiotemporal patterns of burned areas based on the geographic information system for fire risk monitoring," *International Journal of Forestry Research*, vol. 2021, pp. 1–10, 2021. DOI: 10.1155/2021/2784474.

[5] C. P. R. McCarter et al., "Peat fires and legacy toxic metal release: An integrative biogeochemical and ecohydrological conceptual framework," *Earth-Science Reviews*, vol. 256, p. 104 867, 2024. DOI: 10.1016/j.earscirev.2024.104867.

[6] M. Antala, R. Juszczak, C. van der Tol, and A. Rastogi, "Impact of climate change-induced alterations in peatland vegetation phenology and composition on carbon balance," *Science of The Total Environment*, vol. 827, p. 154 294, 2022. DOI: 10.1016/j.scitotenv.2022.154294.

[7] H. Yu, N. Lu, B. Fu, L. Zhang, M. Wang, and H. Tian, "Hotspots, co-occurrence, and shifts of compound and cascading extreme climate events in eurasian drylands," *Environment International*, vol. 169, p. 107 509, 2022. DOI: 10.1016/j.envint.2022.107509.

[8] J. Li, Z. Wang, X. Wu, J. Zscheischler, S. Guo, and X. Chen, "A standardized index for assessing sub-monthly compound dry and hot conditions with application in china," *Hydrology and Earth System Sciences*, vol. 25, no. 3, pp. 1587–1601, 2021. DOI: 10.5194/hess-25-1587-2021.

[9] H. B. Bluestein, F. H. Carr, and S. J. Goodman, "Atmospheric observations of weather and climate," *Atmosphere-Ocean*, vol. 60, no. 3-4, pp. 149–187, 2022. DOI: 10.1080/07055900.2022.2082369.

[10] P. Reiners, J. Sobrino, and C. Kuenzer, "Satellite-derived land surface temperature dynamics in the context of global change—a review," *Remote Sensing*, vol. 15, no. 7, p. 1857, 2023. DOI: 10.3390/rs15071857.

[11] R. Andrade-Pacheco et al., "Finding hotspots: Development of an adaptive spatial sampling approach," *Scientific Reports*, vol. 10, no. 1, p. 10 939, 2020. DOI: 10.1038/s41598-020-67666-3.

[12] Y. Pang et al., "Forest fire occurrence prediction in china based on machine learning methods," *Remote Sensing*, vol. 14, no. 21, p. 5546, 2022. DOI: 10.3390/rs14215546.

[13] Y. Shao et al., "Mapping china's forest fire risks with machine learning," *Forests*, vol. 13, no. 6, p. 856, 2022. DOI: 10.3390/f13060856.

[14] A. D. Syphard, S. J. E. Velazco, M. B. Rose, J. Franklin, and H. M. Regan, "The importance of geography in forecasting future fire patterns under climate change," *Proceedings of the National Academy of Sciences*, vol. 121, no. 32, 2024. DOI: 10.1073/pnas.2310076121.

[15] Y. Cao et al., "Forest fire prediction based on time series networks and remote sensing images," *Forests*, vol. 15, no. 7, p. 1221, 2024. DOI: 10.3390/f15071221.

[16] E. A. Kadir, H. T. Kung, A. A. AlMansour, H. Irie, S. L. Rosa, and S. S. M. Fauzi, "Wildfire hotspots forecasting and mapping for environmental monitoring based on the long short-term memory networks deep learning algorithm," *Environments*, vol. 10, no. 7, p. 124, 2023. DOI: 10.3390/environments10070124.

[17] Y. Michael, D. Helman, O. Glickman, D. Gabay, S. Brenner, and I. M. Lensky, "Forecasting fire risk with machine learning and dynamic information derived from satellite vegetation index time-series," *Science of The Total Environment*, vol. 764, p. 142 844, 2021. DOI: 10.1016/j.scitotenv.2020.142844.

[18] M. Naderpour, H. M. Rizeei, and F. Ramezani, "Forest fire risk prediction: A spatial deep neural network-based framework," *Remote Sensing*, vol. 13, no. 13, p. 2513, 2021. DOI: 10.3390/rs13132513.

[19] Y. Shao et al., "Assessment of china's forest fire occurrence with deep learning, geographic information and multisource data," *Journal of Forestry Research*, vol. 34, no. 4, pp. 963–976, 2023. DOI: 10.1007/s11676-022-01559-1.

[20] N. Imro'ah, N. M. Huda, and A. Y. Pratama, "The implementation of control charts as a verification tool in a time series model for covid-19 vaccine participants in pontianak," *ComTech: Computer, Mathematics and Engineering Applications*, vol. 14, no. 1, pp. 55–67, 2023. DOI: 10.21512/comtech.v14i1.8462.

[21] N. Imro'ah, N. M. Huda, D. S. Utami, T. Umairah, and N. F. Arini, "Control chart for correcting the arima time series model of gdp growth cases," *JTAM (Jurnal Teori Dan Aplikasi Matematika)*, vol. 8, no. 1, p. 312, 2024. DOI: 10.31764/jtam.v8i1.19612.

[22] N. Imro'ah and N. M. Huda, "Control chart as verification tools in time series model," *BAREKENG: Jurnal Ilmu Matematika Dan Terapan*, vol. 16, no. 3, pp. 995–1002, 2022. DOI: 10.30598/barekengvol16iss3pp995-1002.

[23] E. J. Inyang, N. M. Nafo, A. I. Wegbom, and Y. A. Da-Wariboko, "Ets - arima intervention modelling of bangladesh taka/nigerian naira exchange rates," *Science Journal of Applied Mathematics and Statistics*, 2024. DOI: 10.11648/j.sjams.20241201.11.

[24] R. D. Ilmiah and S. I. Oktora, "Arima intervention model for measuring the impact of the lobster seeds fishing and export ban policy on the indonesian lobster export," *Journal of Physics: Conference Series*, vol. 2123, no. 1, p. 012 011, 2021. DOI: 10.1088/1742-6596/2123/1/012011.

[25] E. J. Inyang, E. H. Etuk, N. M. Nafo, and Y. A. Da-Wariboko, "Time series intervention modelling based on esm and arima models: Daily pakistan rupee/nigerian naira exchange rate," *Asian Journal of Probability and Statistics*, vol. 25, no. 3, pp. 1–17, 2023. DOI: 10.9734/ajpas/2023/v25i3560.

[26] S. Dorais, "Time series analysis in preventive intervention research: A step-by-step guide," *Journal of Counseling & Development*, vol. 102, no. 2, pp. 239–250, 2024. DOI: 10.1002/jcad.12508.

[27] N. Imro'ah and N. M. Huda, "Double intervention analysis on the arima model of covid-19 cases in bali," *Journal of the Indonesian Mathematical Society*, vol. 31, no. 1, p. 1347, 2025. DOI: 10.22342/jims.v31i1.1347.